J Therm Spray Tech (2017) 26:1641–1650
DOI 10.1007/s11666-017-0610-1

PEER REVIEWED

Evaporation of Droplets in Plasma Spray–Physical Vapor Deposition Based on Energy Compensation Between Self-Cooling and Plasma Heat Transfer

Mei-Jun Liu[1] · Meng Zhang[1] · Qiang Zhang[1,2] · Guan-Jun Yang[1] · Cheng-Xin Li[1] · Chang-Jiu Li[1]

Submitted: 6 June 2017 / in revised form: 7 July 2017 / Published online: 11 August 2017

Abstract In the plasma spray–physical vapor deposition process (PS-PVD), there is no obvious heating to the feedstock powders due to the free molecular flow condition of the open plasma jet. However, this is in contrast to recent experiments in which the molten droplets are transformed into vapor atoms in the open plasma jet. In this work, to better understand the heating process of feedstock powders in the open plasma jet of PS-PVD, an evaporation model of molten ZrO_2 is established by examining the heat and mass transfer process of molten ZrO_2. The results reveal that the heat flux in PS-PVD open plasma jet (about 10^6 W/m^2) is smaller than that in the plasma torch nozzle (about 10^8 W/m^2). However, the flying distance of molten ZrO_2 in the open plasma jet is much longer than that in the plasma torch nozzle, so the heating in the open plasma jet cannot be ignored. The results of the evaporation model show that the molten ZrO_2 can be partly evaporated by self-cooling, whereas the molten ZrO_2 with a diameter <0.28 μm and an initial temperature of 3247 K can be completely evaporated within the axial distance of 450 mm by heat transfer.

Keywords evaporation · heat flux · heat transfer · PS-PVD · self-cooling

✉ Guan-Jun Yang
ygj@mail.xjtu.edu.cn

[1] State Key Laboratory for Mechanical Behavior of Materials, School of Materials Science and Engineering, Xi'an Jiaotong University, Xi'an 710049, Shaanxi, People's Republic of China

[2] AVIC Beijing Institute of Aeronautical Materials, Beijing 100094, People's Republic of China

Introduction

In the plasma spray–physical vapor deposition (PS-PVD) process, the feedstock powders can not only melt but also vaporize in a high power plasma jet ($\sim$120 kW) with a long plume resulting from the low chamber pressure of 50-200 Pa (Ref 1, 2). Therefore, PS-PVD offers new opportunities to obtain different microstructure coatings, such as lamellar, columnar and mixed coatings (Ref 3). Among the possible coating structures, much attention has been paid to the columnar structure coating deposited by vapor atoms, because it offers excellent thermal shock resistance (Ref 4, 5). The higher gasification degree of feedstock powders is one of the necessary conditions for depositing columnar structure coatings. The gasification degree of the feedstock powders is directly determined by the heating. Therefore, in the PS-PVD process, the heating and evaporating of feedstock powders is the most essential issue.

It has been reported that the heating of feedstock powders takes place predominantly within the plasma torch nozzle (Ref 6). In order to better understand the heating process of feedstock powders, the whole PS-PVD process can be pictured as three steps (Ref 7): (1) the heat exchange process between the feedstock powders and the plasma gas in the plasma torch nozzle, (2) the material transport in the open plasma jet, and (3) the deposition of the coating on the substrate. Initially, the feedstock powders are heated inside the plasma torch nozzle with the heat flux higher than 10^8 W/m^2 (Ref 8). This step results in the formation of molten droplets and vapor atoms. Then, the plasma gas and heated feedstock powders together exit the nozzle and form an open plasma jet under a pressure significantly below the nozzle pressure. The open plasma jet has free molecular flow properties because the *Kn* number is >10 for a

representative particle with a 1 μm diameter (Ref 8). Therefore, there is no significant heating of the feedstock powders in the open plasma jet (Ref 6).

In order to improve the heating and evaporation of the feedstock powders in the plasma torch nozzle, the following studies have been carried out: (1) an improved single cathode vacuum plasma gun (the Sulzer Metco O3CP gun) which allows a total gas flow up to 200 SLPM and power levels up to 180 kW has been used (Ref 1, 9); currently, the O3CP torch nozzle (internal powder feeding method) is generally used for PS-PVD (Ref 1, 8, 9), (2) a higher arc power of about 120 kW is used (Ref 10), (3) a shroud is employed to restrain the expansion of the open plasma jet and to improve the interaction between the plasma gas and the particles (Ref 11, 12), (4) the influence of the plasma gas composition in the particles heating is studied, in which the addition of helium not only concentrates the open plasma jet but also the particle plume due to the high viscosity of helium (Ref 10, 13); the amount of vaporized powder is increased when the plasma gas mixture of argon/hydrogen is replaced by argon/helium (Ref 10), and (5) there is a higher amount of vaporation when using a finer feedstock powders such as agglomerated 7YSZ powders (Metco 6700, Sulzer-Metco; the size ranges from 5 to 22 μm, typically used in PS-PVD) (Ref 14-16). The agglomerated 7YSZ powder (Metco 6700) has a primary particle size ranging from 70 to 130 nm (Ref 7, 14). The agglomerates immediately disintegrated into small primary particles due to weak agglomeration of primary particles during the PS-PVD process (Ref 7, 14, 16). As reported, the transferred enthalpy is sufficient to evaporate particles up to 0.92 μm diameter with the Ar/He plasma (Ref 8). Therefore, large numbers of these fine primary particles can be evaporated in the nozzle (Ref 14). Although the above studies have yielded fruitful results, the feedstock powders have still not been fully evaporated. Therefore, to fully vaporize the spray powders is still a large challenge.

In addition, the influence of spraying distance on the coating structure has also been investigated (Ref 17-19). Different microstructure coatings are achieved by changing the spray distances from 450 to 1400 mm (Ref 17). When the spray distance is extended to 1000 mm, a columnar structure coating deposited from the vapor atoms is obtained. This implies that the YSZ powders are totally vaporized at this spray distance (Ref 17). In other words, the molten droplets can also be transformed into vapor atoms during flight in the open plasma jet. However, this phenomenon is evidently in contrast with those reports in which there is no significant heating to the feedstock powders in the open plasma jet (Ref 6). Therefore, in the PS-PVD process, the heat and the vaporizing process of feedstock powders in the open plasma jet needs further and in-depth understanding.

As reported, the transferred enthalpy inside the O3CP nozzle is sufficient to melt particles of about 2 μm diameter when using the appropriate parameters (Ref 8). Therefore, the primary particles of Metco 6700 powder will completely melt (with at least partial gasification) inside the plasma torch nozzle. However, the plasma jet of PS-PVD expands to about 2 m long and 200-400 mm in diameter due to the low chamber pressure of 50-200 Pa (Ref 1, 2), and the distance from the powder injection position to the nozzle exit is only 10 mm for the O3CP nozzle (Ref 8). Therefore, the transport distance of the molten particles in the open plasma jet is much longer than that in the plasma torch nozzle inside; thus, the heating process of the molten particles at such a long transport distance needs further and in-depth understanding.

In this study, the evaporation process of molten ZrO_2 in the PS-PVD open plasma jet is examined, and an evaporation model of molten ZrO_2 is established for a better understanding of the heat and vaporization process in PS-PVD based on the heat transfer from the open plasma jet and self-cooling heat supply.

Model Development and Experimental Procedures

Model Development

In the plasma torch nozzle, there is a dynamic balance (i.e., the liquid–vapor equilibrium) between liquid and vapor for a molten ZrO_2 at a certain temperature. As shown in Fig. 1(a), the molten ZrO_2 with the plasma gas can exit the plasma torch nozzle at a chamber pressure lower than the nozzle pressure, and then form an open plasma jet. In the open plasma jet, the liquid–vapor equilibrium of the molten ZrO_2 is broken due to the change of the environment conditions such as the surrounding pressure (about 50-200 Pa for PS-PVD) being lower than the plasma torch nozzle pressure, and the heat transfer between the molten ZrO_2 and the plasma gas. Therefore, the processes of the mass and heat transfer may occur when the molten ZrO_2 is transported in the open plasma jet.

The size and the temperature of the molten ZrO_2 are both changed due to the processes of the mass and heat transfer. Therefore, in order to establish the model of evaporation, it is necessary to study the size and temperature change of the molten ZrO_2. The evaporation of the molten ZrO_2 in the open plasma jet is as shown in Fig. 1(b). The basic step of evaporation is the leaving of a molecule (atom or ion) from the liquid phase to the gas phase at the liquid/gas interface. The molecules have a higher energy than a critical level can leave. These high-

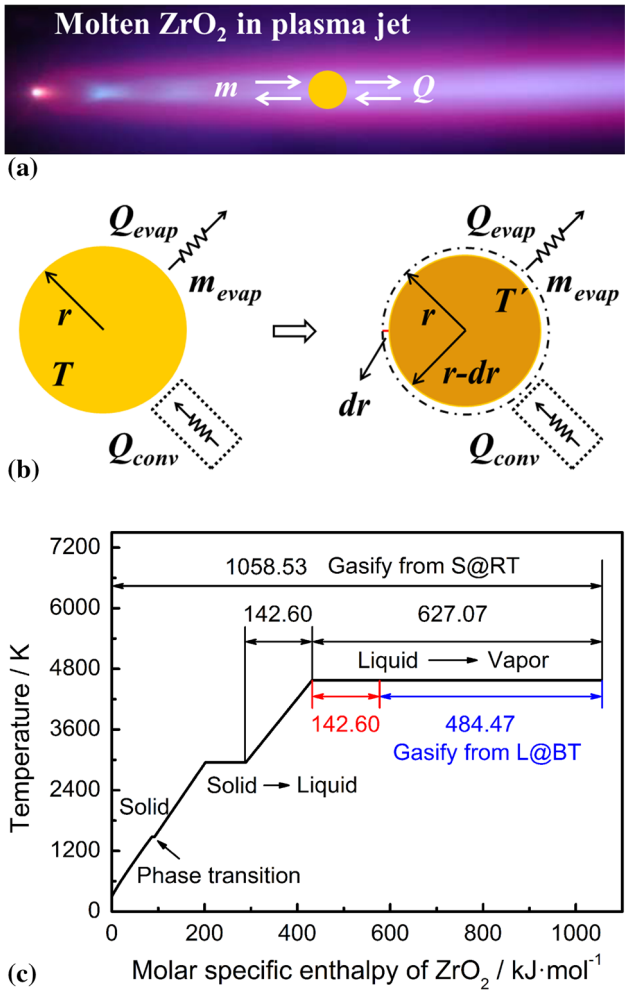

Fig. 1 Schematic of molten ZrO_2 flight in the open plasma jet. (a) The possible process of molten ZrO_2 flight in the open plasma jet, (the plasma jet picture from Ref 1). (b) Schematic of the evaporation process of molten ZrO_2 in the open plasma jet, and (c) the variation of specific enthalpy with temperature of ZrO_2. *S@RT* solid state at room temperature, and *L@BT* liquid state at boiling temperature (here 4500 K)

energy molecules are generated through the fluctuation of the energy state during the change of the environment conditions, such as the decreased surrounding pressure and the outside heating. After this high-energy molecule leaves the liquid phase, the average energy and the size of the residual molten ZrO_2 are decreased. Meanwhile, the outside heating can compensate this energy reduction by heating the liquid. Therefore, the temperature of molten ZrO_2 is changed.

For molten ZrO_2, the evaporation process can be expressed as (Ref 20, 21):

$$ZrO_2(s,l) \rightarrow ZrO(g) + O(g) \quad \text{(Eq 1)}$$

The latent heat of evaporation (Q_0) is 627.07 kJ/mol (Ref 20, 21).

As reported, there is no significant heating of the feedstock powders in the open plasma jet (Ref 6). In this study, for molten ZrO_2, the heating of the open plasma jet could not be ignored. Figure 1(c) shows the enthalpy variation with temperature for ZrO_2 material at a constant pressure of 1 atm as an example. It can be regarded as either a heating process or a cooling process. The heat value required to heat the ZrO_2 from solid state to complete evaporation is about 1058.53 kJ/mol, as shown in Fig. 1(c). At the boiling point, the heat required for the evaporation of the molten ZrO_2 is 627.07 kJ/mol. This only accounts for 59.44% of the heat that required to heat the ZrO_2 from the solid state to evaporation. When the external pressure is reduced from atmospheric pressure to the saturated vapor pressure of melting point, the temperature of the residual particle will decrease. For instance, because of the change of the external pressure, in the process of reducing the residual particles' temperature from 4573 to 2950 K during evaporation, the high-energy molecules are generated by the fluctuation of the energy state as the external pressure decreases, and leaves the liquid phase. The average energy of the residual liquid is decreased and thereby the average temperature of the residual liquid is reduced. In this process, the released energy is about 142.60 kJ/mol. As a result, the actual heat needed for the evaporation of the molten ZrO_2 is 484.47 kJ/mol, accounting for only 45.77% compared to the overall 1058.53 kJ/mol. Therefore, the heat transfer in the open plasma jet might be enough to cause the evaporation of the molten ZrO_2, even if it is not significant.

In order to study the evaporation of molten ZrO_2 in the open plasma jet, the following assumptions are defined:

(1) The pressure of the open plasma jet is equal to the chamber pressure.
(2) The primary ZrO_2 particle is spherical and smaller than 1 μm. The ZrO_2 particle is initially molten (Ref 8). In the open plasma jet, the velocity (833 m/s, Ref 8) of the molten ZrO_2 does not change (Ref 6), the internal temperature is uniform, and the specific heat of molten ZrO_2 is a constant (Ref 22).
(3) The electron emission from the spherical particle surface and the radiation heat transfer are not considered (Ref 8).
(4) The plasma jet expands isentropically (Ref 8).

From Fig. 1(b), the molten ZrO_2 is heated to evaporation by the open plasma jet, whereas the heat is taken away by evaporation. These two processes would cause the temperature of the residual molten ZrO_2 to change. These processes can be written as:

$$m \times C_p \times dT = dQ_{\text{conv}} - dm \times Q_0 \quad \text{(Eq 2)}$$

where m is the residual mass of molten ZrO_2, C_p is the specific heat of molten ZrO_2 ($C_p = 87.864$ J K^{-1} mol^{-1}) (Ref 22), dT is the temperature change of molten ZrO_2 in the heating and evaporation process, dQ_{conv} is the heat transfer by the open plasma jet, dm is the vaporized mass of molten ZrO_2, Q_0 is the latent heat of evaporation of molten ZrO_2.

For the self-cooling controlled evaporation process without considering external heating ($dQ_{conv} = 0$), Eq 2 can be changed to:

$$\frac{m}{m_0} = \exp\left[\frac{C_p}{Q_0} \times (T_0 - T)\right] \quad \text{(Eq 3)}$$

where m_0 is the initial mass of molten ZrO_2, T_0 is the initial temperature of molten ZrO_2, T is the temperature of residual molten ZrO_2.

For the isothermal evaporation process, the heat transferred from the plasma gas to the molten ZrO_2 is used for evaporation:

$$4\pi r_w^2 \times \left(-\frac{\mathrm{d}r_w}{\mathrm{d}t}\right) \times \rho_{pl} \times Q_0 = 4\pi r_w^2 \times \bar{q} \quad \text{(Eq 4)}$$

where r_w is the radius of molten ZrO_2, $\mathrm{d}r_w$ is the radius change of molten ZrO_2 in the heating and evaporation process, ρ_{pl} is the liquid phase density of molten ZrO_2, $\bar{q}$ is the heat flux (W/m^2).

Under PS-PVD conditions, the continuous fluid mechanics method is no longer suitable and the open plasma jet has free molecular flow properties (Ref 8). There is no relationship between heat flux ($\bar{q}$) and radius (r_w) under the free molecular flow condition (Ref 23). Taking $r_w = r_{w0}$ (initial radius) at $t_0 = 0$ (where t is stands for time), it can be obtained that:

$$r_{w,r} = r_{w,0} - K_v t \quad \text{(Eq 5)}$$

K_v is the evaporation constant:

$$K_v = \frac{\bar{q}}{\rho_{pl} \times Q_0} \quad \text{(Eq 6)}$$

here, the averaged, time independent heat flux $\bar{q} = \frac{1}{L_2 - L_1}\int_{z=L_1}^{z=L_2} \bar{q}(z)\mathrm{d}z$ is used, L is the distance of the Z axis.

The heat flux $\bar{q}(z)$ under the condition of free molecular flow can be expressed as (Ref 23)

$$\bar{q}(z) = \bar{q}_a + \bar{q}_i + \bar{q}_e \quad \text{(Eq 7)}$$

where $\bar{q}_a$, $\bar{q}_i$ and $\bar{q}_e$ are the atoms heat flux, the ions heat flux and the electron heat flux, respectively.

For the calculation of heat transfer under the free molecular flow condition, the following additional assumptions have been established by Chen (Ref 24):

(1) complete diffuse reflection of plasma gas particles is assumed at the molten ZrO_2 surface.
(2) heat transfer is treated as a process with steady floating potential on the sphere surface, and the effect of the initial charging process on heat transfer is neglected.
(3) ions recombine with electrons at the sphere surface accompanied by the release of the ionization energy.

It is found that they are almost the same for metallic and nonmetallic materials so that the closed expressions for the metallic case can be applied, for atoms:

$$\begin{aligned}\bar{q}_a &= \frac{Q_a}{4\pi r_w^2} \\ &= \frac{1}{8} a_a n_a \bar{v}_a k_B T_h \left[\left(S_h^2 + \frac{5}{2} - 2\frac{T_w}{T_h}\right)\exp\left(-S_h^2\right)\right. \\ &\quad \left. + \frac{\sqrt{\pi}}{S_h}\left(S_h^4 + 3S_h^2 + \frac{3}{4} - \frac{T_w}{T_h} - 2S_h^2\frac{T_w}{T_h}\right)\mathrm{erf}(S_h)\right]\end{aligned} \quad \text{(Eq 8)}$$

where Q_a is the heat flux from atoms to the whole surface of molten ZrO_2 (W), a_a is the thermal accommodation coefficient of the atoms ($a_a = 1$ is assumed, Ref 8), n_a is the number density of atoms per unit volume, $\bar{v}_a$ is the thermal motion speed of the atoms, $\bar{v}_a = \sqrt{8k_B T_a/\pi m_a}$, k_B is the Boltzmann constant 1.381×10^{-23} J/K, T_a is the temperature of the atoms, m_a is the mass of the atom, S_h is the speed ratio of the feedstock particles and the heavy plasma gas particles (Eq 11), T_w and T_h are the surface temperature of feedstock particles and the temperature of the heavy plasma gas particles, respectively. Under the local thermal equilibrium (LTE) condition, the temperature of all species in the plasma jet is equal to the plasma temperature.

for ions:

$$\begin{aligned}\bar{q}_i &= \frac{Q_i}{4\pi r_w^2} \\ &= \frac{1}{8} a_i n_i \bar{v}_i k_B T_h \left\{\left[\sqrt{\pi}\left(\frac{1}{2S_h} + S_h\right)\mathrm{erf}(S_h) + \exp\left(-S_h^2\right)\right]\right. \\ &\quad \left. \times \left(S_h^2 + \frac{5}{2} - 2\frac{T_w}{T_h} + \frac{E_{ion} - W_s}{a_i k_B T_h} + \frac{e\Phi}{k_B T_h}\right) - \frac{\sqrt{\pi}}{2S_h}\mathrm{erf}(S_h)\right\}\end{aligned} \quad \text{(Eq 9)}$$

where Q_i is the heat flux from ions to the whole surface of the molten ZrO_2 (W), a_i is the thermal accommodation coefficient of the ions ($a_i = 1$ is assumed, Ref 8). n_i is the number density of ions per unit volume. $\bar{v}_i$ is the thermal motion speed of the ions, $\bar{v}_i = \sqrt{8k_B T_i/\pi m_i}$, T_i is the temperature of the ions, m_i is the mass of the ion. E_{ion} is the ionization energy of the plasma gas (for Ar/H$_2$, $E_{ion} = 16.8$ eV, Ref 8). W_s is the electron work function for the feedstock material (for YSZ, $W_s = 4.3$ eV, Ref 25). e is the elementary charge 1.602×10^{-19} C. Φ is the floating potential on the sphere surface (Eq 12).

and for electrons:

$$\bar{q}_e = \frac{Q_e}{4\pi r_w^2} = \frac{1}{4} n_e \bar{v}_e \exp\left(-\frac{e\Phi}{k_B T_e}\right)(2k_B T_e + W_s) \quad \text{(Eq 10)}$$

where Q_e is the heat flux from the electrons to the whole surface of the molten ZrO_2 (W), n_e is the number density of electrons per unit volume. $\bar{v}_e$ is the thermal motion speed of the electrons, $\bar{v}_e = \sqrt{8k_B T_e/\pi m_e}$, T_e is the temperature of the electrons, m_e is the mass of the electrons.

The speed ratio S_h and the floating potential Φ are, respectively, calculated by:

$$S_h = \frac{v_{rel}}{\sqrt{2k_B T_h/m_h}} \quad \text{(Eq 11)}$$

and

$$\Phi = \frac{k_B T_e}{e}\left\{\ln\sqrt{\frac{m_i T_e}{m_e T_i}} - \ln\left[\frac{1}{2}\exp\left(-S_h^2\right) + \frac{\sqrt{\pi}}{4S_h}\left(1 + 2S_h^2\right)\mathrm{erf}(S_h)\right]\right\} \quad \text{(Eq 12)}$$

where v_{rel} is the relative velocity between the plasma gas and molten ZrO_2, moreover, the average velocity of open plasma jet is about 1385 m/s (Ref 6, 8), m_h is the gas particle mass.

Experimental Procedures

Diagnosis of Plasma Condition by Optical Emission Spectrometry

For the above calculations, it is necessary to know the electron number density and the plasma temperature. Therefore, the properties of the open plasma jet are examined by optical emission spectrometry (OES). A Cartesian coordinate system is established to describe the state of open plasma jet, as shown in Fig. 2(a). The light emitted from the open plasma jet is collected by a lens (FC-446-030; Andor Technology, UK), then is transmitted through the optical fiber to the spectrometer, as shown in Fig. 2(b). The plasma spraying parameters in this study are listed in Table 1.

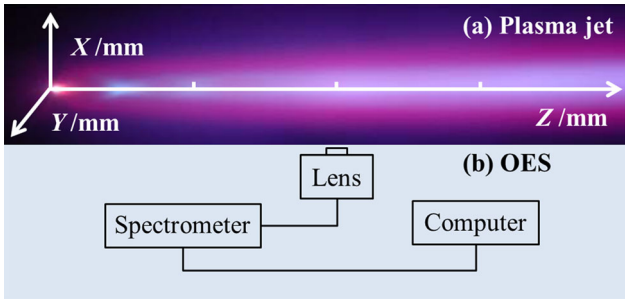

Fig. 2 Cartesian coordinate system of the open plasma jet and emission detection. (a) Cartesian coordinate system of the open plasma jet, (b) OES detection

Electron Number Density

The H_β line of the Balmer series of hydrogen at 486.13 nm is used to calculate the electron number density which is shown to be (Ref 26):

$$\log n_e = 1.452 \log \Delta\lambda_{1/2} + 14.017 \quad \text{(Eq 13)}$$

where n_e (cm^{-3}) is the electron number density and $\Delta\lambda_{1/2}$ (Å) is the full-width at half-maximum (FWHM).

Plasma Temperature

The LTE condition is used as the necessary criterion for the examination of the plasma temperature based on OES. The temperature calculation can be carried out by using the method of double spectral lines (Ref 27, 28):

$$\frac{I_{ji}}{I_{kl}} = \frac{\lambda_{kl} A_{ji} g_j}{\lambda_{ji} A_{kl} g_k} \exp\left(\frac{E_k - E_j}{k_B T}\right) \quad \text{(Eq 14)}$$

where I_{ji} (a.u.) is the spectral intensity generated by the transition from energy level j to i, I_{kl} (a.u.) is the spectral intensity generated by the transition from energy level k to l, λ_{ji} (nm) is the wavelength in the spectrum generated by the transition from energy level j to i, λ_{kl} (nm) is the wavelength in the spectrum generated by the transition from energy level k to l, A_{ji} (s^{-1}) is the Einstein spontaneous transition probability from energy level j to i, A_{kl} (s^{-1}) is the Einstein spontaneous transition probability from energy level k to l, g_j is the statistical weight of energy level j, g_k is the statistical weight of energy level k, E_j (eV) is the excitation energy of energy level j, E_k (eV) is the excitation energy of energy level k.

Results and Discussion

The Evaporation Process of Molten ZrO_2 Controlled by Self-Cooling

In order to better understand the temperature reduction of molten ZrO_2 via the latent heat of evaporation, the

Table 1 Plasma spraying parameters

Parameter	Unit	Value
Power	kW	60
Current	A	750
Chamber pressure	Pa	100
Ar flow	slpm	60
H_2 flow	slpm	12
Z axial detection distance	mm	50/90/180/270/360/450
Feedstock powder		Metco 6700 (Sulzer-Metco)
Powder feed rate	g/min	0.5

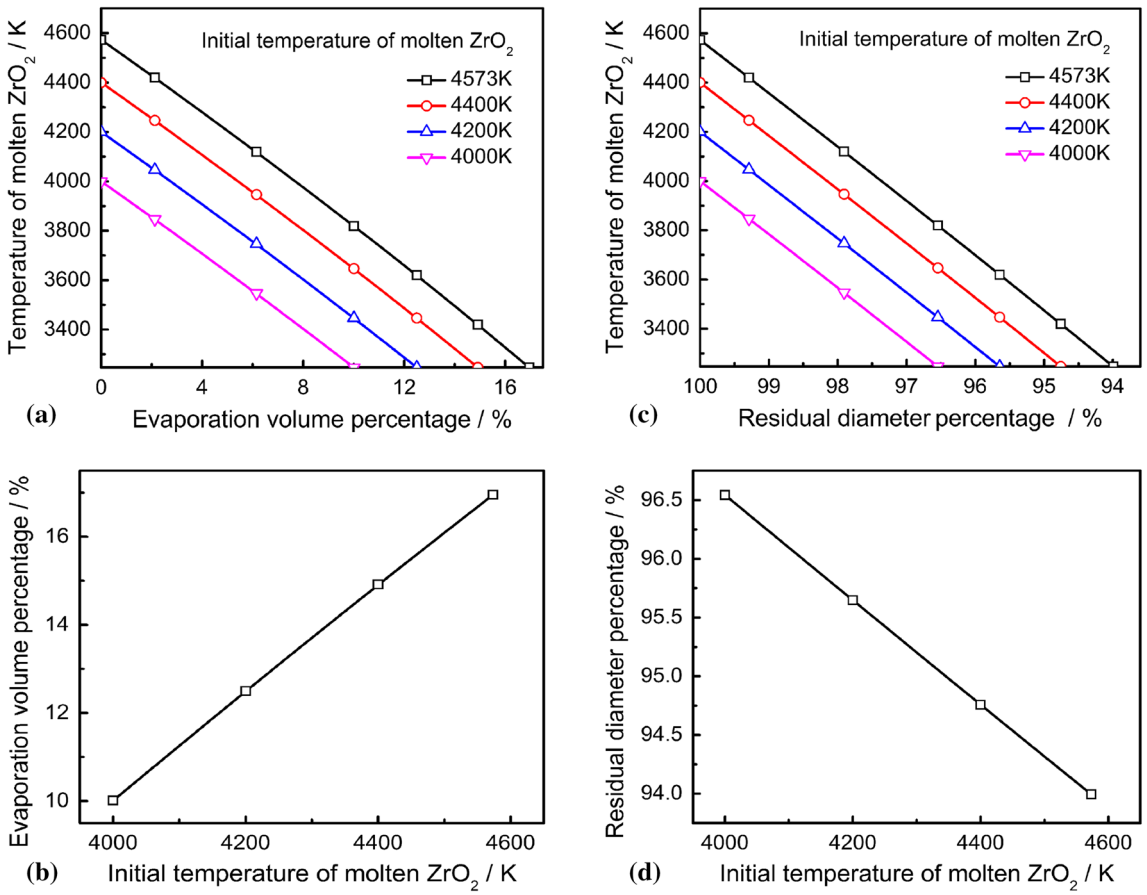

Fig. 3 The change of temperature along with total evaporation volume and diameter decrease, respectively. The initial temperatures of molten ZrO_2 are 4573, 4400, 4200 and 4000 K, respectively

evaporation process without considering external heating ($dQ_{conv} = 0$) is studied first. The molten ZrO_2 with different initial temperatures are selected.

Figure 3(a) and (b) shows the influence of the initial molten ZrO_2 temperature on total evaporation volume during evaporation. According to Eq 3, there is an exponential relationship between the mass evolution and the temperature. However, the exponential slopes of the curve as shown in Fig. 3 are not obvious due to the higher latent heat of evaporation of ZrO_2 ($Q_0 = 627.07$ kJ/mol). At a certain initial temperature such as 4573 K as shown in Fig. 3(a), the total evaporation volume of molten ZrO_2 is increased as the evaporation process proceeds. At the same time, the latent heat of evaporation is taken away and results in the decrease of the residual molten ZrO_2 temperature. As given in Fig. 3(b), the total evaporation volume is increased with the rise of the initial molten ZrO_2 temperature. The total evaporation volume fraction reaches 17% when the initial molten ZrO_2 temperature is 4573 K. Those results indicate that the higher initial molten ZrO_2 temperature will provide more latent heat of evaporation, and generate more total evaporation volume.

Figure 3(c) and (d) shows the influence of the initial molten ZrO_2 temperature on residual diameter during evaporation. It can be seen from Fig. 3(c) that the size of the molten ZrO_2 is decreased in the evaporation process. The higher initial molten ZrO_2 temperature can provide more latent heat of evaporation. This leads to a larger evaporation volume, and smaller residual diameter. Meanwhile, the evaporation process will reduce the temperature of the molten ZrO_2, and it is stopped when the temperature drops to 3247 K.

The above results indicate that the molten ZrO_2 can be partly transformed into vapor atoms due to the latent heat of evaporation offered by the temperature decrease of residual molten ZrO_2, even if there is no significant external heating in the open plasma jet of PS-PVD. Therefore, the size and temperature of the molten ZrO_2 will be decreased in the evaporation process during the initial temperature higher than at the saturated vapor pressure of molten ZrO_2.

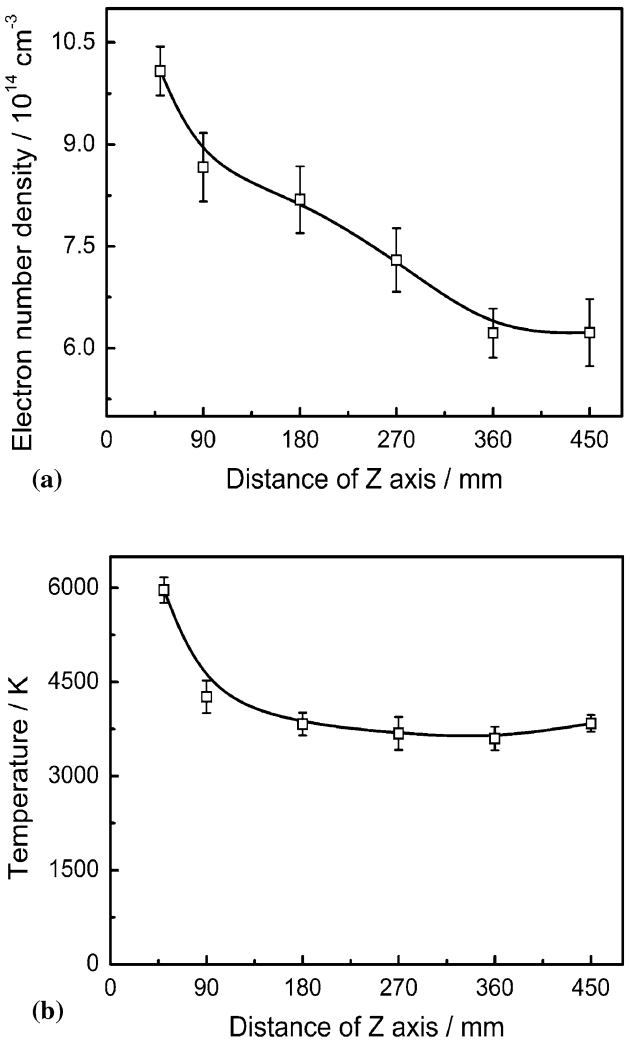

Fig. 4 The distribution of the electron number density (a) and plasma temperature (b) along the *Z* axial direction of the plasma jet

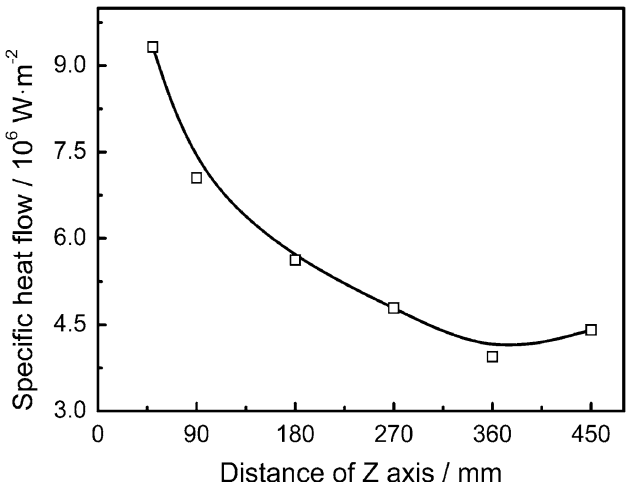

Fig. 5 The distribution of heat flux along the *Z* axial direction of the open plasma jet, the initial temperature is 3247 K

The Evaporation Process of Molten ZrO_2 with External Heated

In order to study the heating of molten ZrO_2 by plasma jet, the characteristics of the open plasma jet are researched first. The distribution of the electron number density is shown in Fig. 4(a). The electron number density is decreased significantly from 10^{15} cm^{-3} to 6×10^{14} cm^{-3} as the axial distance ranges from 50 to 450 mm with the expansion of the plasma jet, as observed in Fig. 4(a).

In the PS-PVD process, the LTE condition is necessary for finding the plasma temperature by OES detection. The local thermal equilibrium condition is usually defined as the electron number density of the plasma reaching a critical value. According to the formula given by Griem (Ref 29), this critical electron number density value can be estimated to 4.2×10^{14} cm^{-3}, which is comparable to that shown in Fig. 4(a). Therefore, the open plasma jet in this work can be regarded as being in a local thermal equilibrium state, and the temperature of these species (such as electron, atoms and ions) in the plasma jet are assumed to be equal (Ref 30).

The distribution of plasma temperature is given in Fig. 4(b). It can be seen that the plasma temperature decreases sharply and then stays steady when the axial distance ranges from 50 to 450 mm. The plasma temperature is above 3500 K, and it is higher than the melting point of ZrO_2. The plasma temperature is not affected by the feedstock powders injection reported in our previous study (Ref 31).

The heat flux transferred by the plasma gas to the molten ZrO_2 is calculated by the electron number density and the plasma temperature, and the result is plotted in Fig. 5. As shown in Fig. 5, the heat flux is changed along the axial direction. The variation of the heat flux ranges from 9×10^6 to 4×10^6 W/m^2 with the axial distance increasing from 50 to 450 mm. Furthermore, this indicates that the heat flux in the whole open plasma jet is smaller than in the plasma torch nozzle (about 10^8 W/m^2, Ref 8). The averaged values of $\bar{q}$ in different distance ranges of the *Z* axis are calculated, and the values are 8.2×10^6, 6.3×10^6, 5.2×10^6, 4.4×10^6 and 4.2×10^6 $W\ m^2$ corresponding to 50-90, 90-180, 180-270, 270-360 and 360-450 mm of *Z* axial ranges, respectively.

The enthalpy transferred to spherical particles is plotted in Fig. 6 as a function of the particle diameter; the horizontal lines indicate the latent heat of evaporation. Because the small particles have a larger specific surface than larger particles, the heat transfer coefficient of the small particles is higher than the larger particles. It can be seen from Fig. 6(a) that the smaller the particle size, the higher the

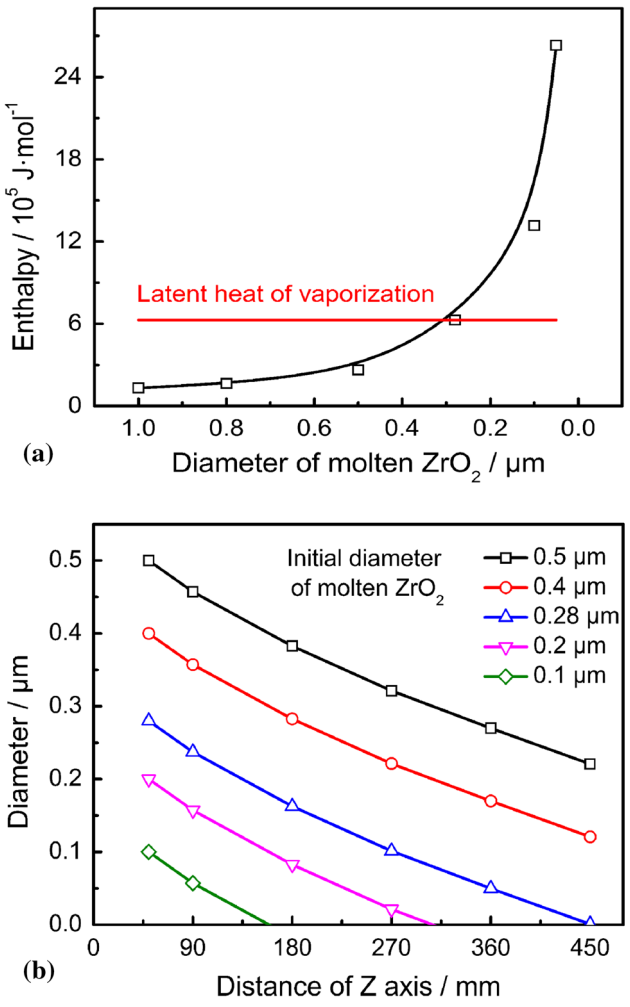

Fig. 6 Enthalpy transferred to molten ZrO_2 as function of the diameter (a) and the change of molten ZrO_2 size along the *Z* axial direction of the open plasma jet (b), The initial temperature is 3247 K

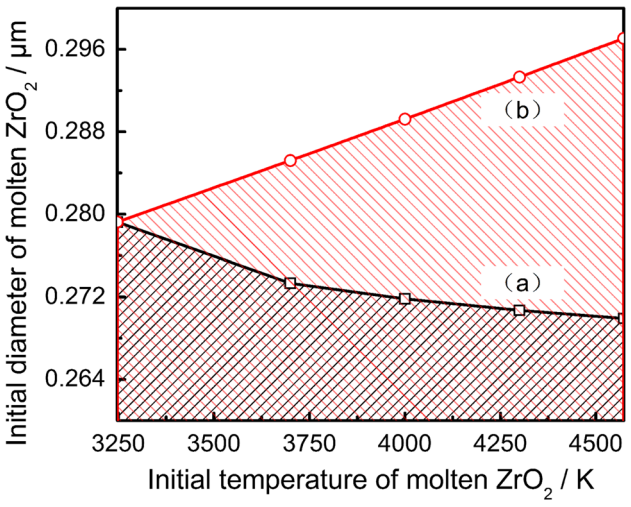

Fig. 7 The initial temperature required for the complete evaporation of molten ZrO_2 with different diameters, (a) without considering the effect of self-cooling, just the effect of heat transfer, (b) considering the effect of self-cooling and heat transfer

heat transfer. It is obvious that the transferred enthalpy is sufficient to evaporate the molten ZrO_2 up to 0.28 μm in diameter.

Figure 6(b) shows the variation of molten ZrO_2 size along the *Z* axial distance. In the open plasma jet, the size of the molten ZrO_2 decreases as the evaporation process proceeds. The small molten ZrO_2 of less than (or equal to) 0.28 μm can be completely evaporated at the *Z* axial distance of <450 mm. In contrast, it might be completely evaporated at a greater distance with the size of the molten ZrO_2 above 0.28 μm.

According to the above analysis, although the heat flux in the whole open plasma jet is smaller than that in the plasma torch nozzle, the heat in the open plasma jet cannot be ignored because the distance of the molten ZrO_2 flying in open plasma jet is much longer than in the plasma torch nozzle.

Conditions of Complete Evaporation in the Open Plasma Jet

Figure 7 shows the initial temperature required for the complete evaporation of molten ZrO_2 in different diameters. It can be found that the size of molten ZrO_2 below the black curve (Fig. 7a) can be completely evaporated within the axial distance of 450 mm. In contrast, the molten ZrO_2 size above the black curve cannot be completely evaporated within the *Z* axial distance of 450 mm and it might be completely evaporated at a greater distance. From Fig. 7, simultaneously considering the effect of self-cooling and heat transfer, the size of the molten ZrO_2 below the red curve (Fig. 7b) can be completely evaporated within the *Z* axial distance of 450 mm. In contrast, the molten ZrO_2 size above the red curve cannot be completely evaporated within the *Z* axial distance of 450 mm. This obviously indicates that the self-cooling of molten ZrO_2 can become larger with evaporation.

According to all the above results, the evaporation process of molten ZrO_2 can be described as follows. The feedstock powders are heated in the plasma torch nozzle, forming molten ZrO_2. The molten ZrO_2 exits the nozzle along with the plasma gas. In the open plasma jet, the pressure is much lower than in the nozzle. Therefore, the liquid–vapor equilibrium of the molten ZrO_2 is broken, and the evaporation process begins. The size and temperature of the molten ZrO_2 are decreased in the evaporation process because the mass and latent heat of evaporation are taken away. Furthermore, the heat needed for evaporation is provided by the heat transfer from the plasma jet, thus the evaporation process continues until the evaporation is

completely finished. Therefore, the molten ZrO_2 can be partially or even totally transformed into vapor atoms while in the open plasma jet.

Conclusions

In the open plasma jet of PS-PVD, the evaporation process of molten ZrO_2 has been studied, and the evaporation mode of molten ZrO_2 demonstrated. The main conclusions are as follows:

(1) The molten ZrO_2 can be partly evaporated by self-cooling. The total evaporation volume is determined by the initial temperature of the molten ZrO_2. The higher initial temperature can provide more latent heat of evaporation, and result in more total evaporation volume and smaller residual size. The evaporation process takes away the heat and leads to the decrease in the temperature of the residual molten ZrO_2.

(2) In the whole open plasma jet, the heat flux transferred from the plasma gas to the molten ZrO_2 is about 10^6 W/m^2, which is smaller than that in the nozzle (about 10^8 W/m^2); however, the flying distance of the molten ZrO_2 in the open plasma jet is much longer than in the nozzle, so the heating in the jet cannot be ignored.

(3) The results of the evaporation model show that the molten ZrO_2 with a diameter of <0.28 μm and an initial temperature of 3247 K can be completely evaporated within the axial distance of 450 mm.

Acknowledgments This project was supported by the National Basic Research Program of China (No. 2013CB035701), the Fundamental Research Funds for the Central Universities, and the National Program for Support of Top-notch Young Professionals.

References

1. K. von Niessen, M. Gindrat, and A. Refke, Vapor Phase Deposition Using Plasma Spray-PVD (TM), *J. Therm. Spray Technol.*, 2010, **19**(1-2), p 502-509
2. K. von Niessen and M. Gindrat, Plasma Spray-PVD: A New Thermal Spray Process to Deposit Out of the Vapor Phase, *J. Therm. Spray Technol.*, 2011, **20**(4), p 736-743
3. D. Zhu, H.T. Lin, Y. Zhou et al., Plasma Spray-Physical Vapor Deposition (PS-PVD) of Ceramics for Protective Coatings, *Ceram. Eng. Sci. Proc.*, 2011, **32**(3), p 73-84
4. M. Goral, S. Kotowski, A. Nowotnik, M. Pytel, M. Drajewicz, and J. Sieniawski, PS-PVD Deposition of Thermal Barrier Coatings, *Surf. Coat. Technol.*, 2013, **237**, p 51-55
5. S. Rezanka, G. Mauer, and R. Vassen, Improved Thermal Cycling Durability of Thermal Barrier Coatings Manufactured by PS-PVD, *J. Therm. Spray Technol.*, 2014, **23**(1-2), p 182-189
6. G. Mauer, M.O. Jarligo, S. Rezanka, A. Hospach, and R. Vassen, Novel Opportunities for Thermal Spray by PS-PVD, *Surf. Coat. Technol.*, 2015, **268**, p 52-57
7. G. Mauer, A. Hospach, N. Zotov, and R. Vassen, Process Conditions and Microstructures of Ceramic Coatings by Gas Phase Deposition Based on Plasma Spraying, *J. Therm. Spray Technol.*, 2013, **22**(2-3), p 83-89
8. G. Mauer, Plasma Characteristics and Plasma-Feedstock Interaction Under PS-PVD Process Conditions, *Plasma Chem. Plasma Process.*, 2014, **34**(5), p 1171-1186
9. M. Gindrat, H.-M. Höhle, K. Niessen, P. Guittienne, D. Grange, and C. Hollenstein, Plasma Spray-CVD: A New Thermal Spray Process to Produce Thin Films from Liquid or Gaseous Precursors, *J. Therm. Spray Technol.*, 2011, **20**(4), p 882-887
10. G. Mauer, A. Hospach, and R. Vassen, Process Development and Coating Characteristics of Plasma Spray-PVD, *Surf. Coat. Technol.*, 2013, **220**, p 219-224
11. Q.Y. Chen, C.X. Li, J.Z. Zhao, G.J. Yang, and C.J. Li, Microstructure of YSZ Coatings Deposited by PS-PVD Using 45 kW Shrouded Plasma Torch, *Mater. Manuf. Process*, 2016, **31**(9), p 1183-1191
12. Q.Y. Chen, C.X. Li, T. Wei, H.B. Sun, S.L. Zhang, X.T. Luo, G.J. Yang, C.J. Li, and M.L. Liu, Controlling Grain Size in Columnar YSZ Coating Formation by Droplet Filtering Assisted PS-PVD Processing, *RSC Adv.*, 2015, **5**(124), p 102126-102133
13. J. Aubreton, M.F. Elchinger, V. Rat, and P. Fauchais, Two-Temperature Transport Coefficients in Argon Helium Thermal Plasmas, *J. Phys. D Appl. Phys.*, 2003, **37**(1), p 34-41
14. A. Hospach, G. Mauer, R. Vassen, and D. Stoever, Characteristics of Ceramic Coatings Made by Thin Film Low Pressure Plasma Spraying (LPPS-TF), *J. Therm. Spray Technol.*, 2012, **21**(3-4), p 435-440
15. B. Vautherin, M.P. Planche, R. Bolot, A. Quet, L. Bianchi, and G. Montavon, Vapors and Droplets Mixture Deposition of Metallic Coatings by Very Low Pressure Plasma Spraying, *J. Therm. Spray Technol.*, 2014, **23**(4), p 596-608
16. X.F. Zhang, K.S. Zhou, C.M. Deng, M. Liu, Z.Q. Deng, C.G. Deng, and J.B. Song, Gas-Deposition Mechanisms of 7YSZ Coating Based on Plasma Spray-Physical Vapor Deposition, *J. Eur. Ceram. Soc.*, 2016, **36**(3), p 697-703
17. C. Li, H. Guo, L. Gao, L. Wei, S. Gong, and H. Xu, Microstructures of Yttria-Stabilized Zirconia Coatings by Plasma Spray-Physical Vapor Deposition, *J. Therm. Spray Technol.*, 2015, **24**(3), p 534-541
18. L. Gao, H. Guo, L. Wei, C. Li, S. Gong, and H. Xu, Microstructure and Mechanical Properties of Yttria Stabilized Zirconia Coatings Prepared by Plasma Spray Physical Vapor Deposition, *Ceram. Int.*, 2015, **41**(7), p 8305-8311
19. L. Gao, H. Guo, L. Wei, C. Li, and H. Xu, Microstructure, Thermal Conductivity and Thermal Cycling Behavior of Thermal Barrier Coatings Prepared by Plasma Spray Physical Vapor Deposition, *Surf. Coat. Technol.*, 2015, **276**, p 424-430
20. W.A. Chupka, J. Berkowitz, and M.G. Inghram, Thermodynamics of the Zr-ZrO_2 System: The Dissociation Energies of ZrO and ZrO_2, *J. Chem. Phys.*, 1957, **26**(5), p 1207-1210
21. E. Murad and D.L. Hildenbrand, Thermochemical Properties of Gaseous ZrO and ZrO_2, *J. Chem. Phys.*, 1957, **63**(65), p 1133-1139
22. http://kinetics.nist.gov/janaf/html/O-053.html
23. X. Chen, J. Chen, and Y. Wang, Unsteady Heating of Metallic Particles in a Rarefied Plasma, *Plasma Chem. Plasma Process.*, 1995, **15**(2), p 199-219
24. X. Chen and P. He, Heat Transfer from a Rarefied Plasma Flow to a Metallic or Nonmetallic Particle, *Plasma Chem. Plasma Process.*, 1986, **6**(4), p 313-333

25. U. Vohrer, H.D. Wiemhöfer, W. Göpel, V. Hassel, and A.J. Burggraaf, Electronic Properties of Ion-Implanted Yttria-Stabilized Zirconia, *Solid State Ionics*, 1993, **59**(1-2), p 141-149
26. N. Zhang, F. Sun, L. Zhu, M.P. Planche, H. Liao, C. Dong, and C. Coddet, Electron Temperature and Density of the Plasma Measured by Optical Emission Spectroscopy in VLPPS Conditions, *J. Therm. Spray Technol.*, 2011, **20**(6), p 1321-1327
27. J.H. Cui, Z.F. Xu, and J.L. Zhang, Online Diagnosis of Electron Excitation Temperature in $CH_4 + H_2$ Discharge Plasma at Atmospheric Pressure by Optical Emission Spectra, *Sci. China Phys. Mech. Astron.*, 2008, **51**(12), p 1892-1896
28. N. Zhang, F. Sun, L. Zhu, C. Verdy, and M.P. Planche, Characteristics of Cu Film Deposited Using VLPPS, *J. Therm. Spray Technol.*, 2011, **20**(1), p 351-357
29. H. Griem, *Plasma Spectroscopy*, McGraw-Hill Book Company, New York, 1964
30. L. Torrisi, F. Caridi, D. Margarone, and A. Borrielli, Characterization of Laser-Generated Silicon Plasma, *Appl. Surf. Sci.*, 2008, **254**(7), p 2090-2095
31. Q.Y. Chen, X.Z. Peng, G.J. Yang, C.X. Li, and C.J. Li, Characterization of Plasma Jet in Plasma Spray-Physical Vapor Deposition of YSZ Using a <80 kW Shrouded Torch Based on Optical Emission Spectroscopy, *J. Therm. Spray Technol.*, 2015, **24**(6), p 1038-1045